Applications of Remote Sensing to Agrometeorology

Proceedings of a Course held at the
Joint Research Centre of the
Commission of the European Communities
in the Framework of the ISPRA-Courses,
Ispra, Varese, Italy, 6-10 April 1987

Edited by

F. Toselli

ISPRA Courses on Remote Sensing

Kluwer Academic Publishers

EXTRACTION OF SURFACE TEMPERATURE FROM SATELLITE DATA

Hartmut Grassl
GKSS-Forschungszentrum Geesthacht GmbH
Max-Planck-Strasse
D-2054 Geesthacht - Fed. Rep. of Germany

ABSTRACT. The surface temperature figures in nearly all equations for energy fluxes through a surface element. It is routinely derived from satellite radiances over the oceans. However, over land the changing surface emissivity, strong daytime heating as well as nighttime cooling and the difficulty of defining surface temperature for a canopy, have prevented a routine application. This paper shows the possible influences of water vapour content, near surface thermal structure, aerosol particles, thin clouds, slant paths and surface emissivity on the correction of atmospheric masking. A procedure for land surface temperature determination for the NOAA 7, 9 satellite data comprising four steps is put forward:
- water surface temperature derivation;
- interpolation of the water surface correction;
- additional correction due to heated or cooled surfaces;
- choice of the highest temperature from the three thermal IR channels.

The procedure is applied to a daytime and a nighttime scene covering the Alps.

1. INTRODUCTION

All fluxes determining the energy budget of a surface element, except solar radiation flux, involve - if parameterized - the surface temperature, either directly like longwave net flux or indirectly via a temperature gradient like sensible heat flux and latent heat flux into the atmosphere as well as the sensible heat flux into the soil. Therefore, the two-dimensional surface temperature distribution is needed, whenever the total energy budget or parts of it are sought for any area. Since the direct measurement of surface skin temperature is impossible (due to the disturbance by any thermometer) an ideal means is the radiometric determination of temperature via surface emission within the thermal infrared spectrum from an airplane or a satellite.

Immediately two error sources come into play:
- the non-blackness of all natural surfaces;
- the emission of the atmosphere between the measuring platform and the

F. Toselli (ed.), Applications of Remote Sensing to Agrometeorology, 199–220.

surface at temperatures differing from the surface temperature.

Both errors vary with time for a distinct surface element. In both cases this is mainly caused by changes in water content either by a change from a dry to a wet surface or by changes in atmospheric water vapour.

Since the atmosphere has no perfect spectral window in the thermal infrared, a one-channel radiometer for the remote measurement of surface temperature may at best apply a climatological mean correction of the atmosphere's masking, if no calibration points are available.

This lecture will give - after a short section on theory - an account of surface parameters, gases and aerosol particle characteristics influencing the remote measurement of surface temperature, will then show algorithms to establish a stand-alone remote surface temperature measurement, and will finally discuss a variety of applications of different algorithms also including the daily temperature amplitude determination.

2. ESSENTIAL PHYSICAL BACKGROUND

2.1 Governing Equations

Remote sensing by electromagnetic waves in the visible and infrared part of the spectrum normally applies time averages over many waves. The appropriate equation governing the time averaged squares of amplitudes of electromagnetic waves is the radiative transfer equation.

Written for spectral radiance I_λ, the energy flowing through a unit surface from a unit space angle per unit time and unit spectral interval (here wavelength λ; thus the dimension is $Wm^{-2}sr^{-1}\mu m^{-1}$)

$$\frac{dI_\lambda}{d\tau_\lambda} = - I_\lambda + J_\lambda$$

or

$$\frac{dI_\lambda}{ds} = (-I_\lambda + J_\lambda) \cdot e_\lambda \qquad (1)$$

It simply states that firstly the incoming spectral radiance I_λ reduces more for a greater spectral optical depth increment $d\tau_\lambda$ of a medium, and that secondly I_λ may be increased by a source J_λ. The spectral optical depth τ_λ is defined here as the integral over spectral volume extingtion coefficient e_λ along a distinct direction s

$$\tau_\lambda = \int_0^{s^*} e_\lambda \, ds \qquad (2)$$

For thermal infrared remote sensing the integration of Eq.(1) (an integro-differential equation in scattering media) may be simplified con-

siderably by neglecting scattering in the atmosphere, thus reducing the spectral source J_λ to Planck's function B_λ, which merely depends on temperature T. This simplification is a good approximation for all cloudless areas in the thermal infrared outside very strong atmospheric turbidity layers. As a rule of thumb the scattering optical depth caused by aerosols is by a factor of 5 smaller in the main thermal infrared window from 10-30 µm wavelength as compared to the visible wavelength, where $\tau_{aerosol} < 0.2$ is mostly satisfied.

After a formal integration along a distinct path in a non-scattering atmosphere, here from $\tau_\lambda = 0$ at the top of the atmosphere - where as a boundary condition no emission from space is assumed, i.e. $I_\lambda^- = 0$ - to the ground with total optical depth τ_λ^*, we obtain for the spectral radiance I_λ^+ emerging at the top of the atmosphere

$$I_\lambda^+ = \varepsilon_\lambda B_\lambda(T_s) e^{-\tau_\lambda^*} \qquad \text{surface contribution}$$

$$+ \int_0^{\tau_\lambda^*} B_\lambda T(\tau_\lambda) e^{-\tau_\lambda} d\tau_\lambda \qquad \text{atmospheric emission} \qquad (3)$$

$$+ (1-\varepsilon_\lambda) \int_{\tau_\lambda^*}^{0} B_\lambda(T(\tau_\lambda)) e^{-\tau_\lambda} d\tau_\lambda e^{-\tau_\lambda^*} \qquad \text{surface reflection of downwelling emission of the atmosphere (here written for a smooth surface only)}$$

Only the first term on the right side contains information on surface temperature T_s via Planck's function $B_\lambda(T_s)$; ideally the spectral emissivity ε_λ reaches unity for a blackbody. Fortunately, most natural surfaces, especially water and vegetated surfaces, reach $\varepsilon_\lambda > 0.95$, even $\varepsilon_\lambda \cong 0.99$ in thermal infrared windows. In order to obtain the spectral surface emission $\varepsilon_\lambda B_\lambda(T_s)$ to the satellite spectral transmission $t_\lambda = e^{-\tau_\lambda}$ of the atmosphere should be as small as possible, i.e. only atmospheric windows are suitable wavelength positions.

The second term, atmospheric emission, masks the surface contribution. If near surface layers of the atmosphere with $B_\lambda T(\tau_\lambda)$ only slightly smaller than $B_\lambda(T_s)$ constitute the main part of the integral of the second term, the transmission loss of surface emission in term number one is to a large extent compensated. However, this is not at all the case for high aerosol particle layers or subvisible cirrus clouds both emitting at low tempeatures. In this case even very small spectral optical depth values with $\tau_\lambda \leq 0.01$ may cause up to one percent error in spectral upward radiance I_λ^+, which at ambient temperatures of 20°C is approximately equivalent to a one degree temperature error if measuring in the 10-13 µm central infrared window. Since vertical temperature and humidity structure (water vapour absorption is the dominant absorption in the windows) vary considerably depending on weather conditions and geographical position the degree of compensation mentioned above also varies, leaving a variety of necessary corrections for the atmosphere's masking ranging from no correction to up to 10 K.

The third term accounts for the reflection of downwelling thermal

infrared radiances by the surface. Its importance decreases with increasing ε_λ and extinction by the atmosphere; thus it is nearly negligible over water surfaces in the tropics and it becomes considerable in moderately humid atmospheres over rock surfaces. If handled accurately for a rough surface, either composed of surface elements with different slopes or vegetated, this term needs a proper description of spectral emissivity ε_λ as a function of both the angle of incidence of downwelling radiance and the surface element slope distribution. Its effect is a partial compensation of the blackbody emissivity deficit in term number one, with growing compensation for increasing surface roughness.

2.2 Relation to Temperature

The quantity desired is the surface temperature T_S and it is hidden in the spectral Planck's function $B_\lambda(T_S)$. Any upwelling spectral radiance I_λ^+, the satellite signal, may be expressed in a so-called brightness temperature T_B, which merely is a temperature a blackbody emitting the same spectral radiance would have. The simple inversion of Planck's law

$$B_\lambda(T)d_\lambda = \frac{2hc^2}{\lambda^5} \cdot \frac{1}{e^{hc/\lambda T} - 1} d\lambda \qquad (4a)$$

$$B_\nu(T)d_\nu = \frac{2h\nu^3}{c^2} \cdot \frac{1}{e^{\nu h/kT} - 1} d\lambda \qquad (4b)$$

(if written for wave-number $\nu = 1/\lambda$ in spectroscopy)
h = Planck's constant;
c = velocity of light;
k = Boltzmann's constant;

gives brightness temperature T_B

$$T_B = \frac{a}{\ln B_\nu(T) - b}; \quad a = c_2\nu, b = \ln c_1\nu^3, \quad c_1 = 2h/c^2, c_2 = h/k \qquad (5)$$

The conversion of satellite signals I_λ^+ into brightness temperatures T_B is generally accepted. However, these values are often erroneously used directly as surface temperatures before the atmospheric masking has been corrected. Before these corrections we will introduce Eq.(3) and also Eq.(5) which, when written for the monochromatic idealization, must be adapted to the finite spectral width of a radiometer channel.

2.3 Account of the Finite Spectral Width

The width of satellite radiometer channels causes a modification of the idealized equations (3) and (5). If the normalized spectral transmission $\varphi^*(\nu)$ or $\varphi^*(\lambda)$, for which we have

$$\int_{\nu_1}^{\nu_2} \varphi^*(\nu)\,d\nu = \int_{\lambda_1}^{\lambda_2} \varphi^*(\lambda)\,d\lambda = 1 \qquad (6)$$

is introduced into Eq.(3) the real satellite signal becomes

$$I^+_{\Delta\nu} = \int_{\nu_1}^{\nu_2} I^+_\nu \cdot \varphi^*(\nu)\,d\nu = \int_{\nu_1}^{\nu_2} B_\nu(T_B) \cdot \varphi^*(\nu)\,d\nu$$
$$I^+_{\Delta\lambda} = \int_{\lambda_1}^{\lambda_2} I^+_\lambda \cdot \varphi^*(\lambda)\,d\lambda = \int_{\lambda_1}^{\lambda_2} B_\lambda(T_B) \cdot \varphi^*(\lambda)\,d\lambda \qquad (7)$$

with:
ν_1, ν_2 = wavenumber for which $\varphi^*(\nu) = 0$ if $\nu < \nu_1$ and $\nu > \nu_2$;
λ_1, λ_2 = wavelength for which $\varphi^*(\lambda) = 0$ if $\lambda < \lambda_1$ and $\lambda > \lambda_2$.

Since $\varphi^*(\nu)$ cannot be simply expressed as an analytical function, Eq.(7) cannot be exactly - as Eq.(5) - converted into a brightness temperature T_B. Following an empirical approach by Singh (1984) the brightness temperature T_B of existing satellite radiometer channels is sufficiently accurate if described by

$$T_B = a_1 + b_1 \cdot T'_B \qquad (8)$$

where the so-called preliminary brightness temperature T'_B is related to $I^+_{\Delta\nu}$ as follows

$$T'_B = \frac{b_2}{\ln I^+_{\Delta\nu} - a_2} \quad \text{(equivalent to Eq.(5))} \qquad (9)$$

This approach also accounts - in Eq.(8) - for any occurring non-linear calibration curves of a satellite radiometer.

As an example, Table I displays the coefficients for all three thermal infrared channels with central wavelengths $\bar{\lambda}$ at 3.7, 11 and 12 µm of the NOAA 7 polar orbiting satellite, the first to contain the split-window at 11 and 12 µm.

2.4 ΔT for Different Atmospheres

The dependence of the temperature correction ΔT on different situations is best explained by showing ΔT for variations of spectral emissivity ε_λ, water vapour content, temperature structure, viewing angle, aerosol particle optical depth and optically thin, undetected clouds.

The best way of obtaining an overview of possible corrections is

TABLE I
Coefficients in Eqs.(8) and (9) needed for the determination of T_B for the Advanced Very High Resolution Radiometer (AVHRR) infrared channels onboard the NOAA 7 satellite

Channel	$\bar{\lambda}$	a_1 K	b_1	a_2	b_2 K
3	3.7 μm	0	1	12.2554	-3821.046
4	11 μm	-12.920	1.045	9.2058	-1344.832
5	12 μm	- 7.717	1.027	8.9373	-1226.189

by numerical simulations with a radiative transfer model. The following results were all available before a procedure for land surface temperature determination had been devised.

2.4.1 Emissivity dependence. Within the $0.95 < \varepsilon_{\Delta\lambda} < 1.0$ range of mean surface emissivity $\varepsilon_{\Delta\lambda}$ for the wavelength band $\Delta\lambda$ of a radiometer channel, the temperature correction ΔT used to infer surface temperature T_S by

$$T_S = T_B + \Delta T \tag{10}$$

is nearly linearly dependent on the deviation from the blackbody emission $1-\varepsilon_{\Delta\lambda}$ with $\Delta T/\Delta\varepsilon_{\Delta\lambda} = -0.45$ K for one percent change in mean emissivity $\varepsilon_{\Delta\lambda}$. Moreover, $\Delta T/\Delta\varepsilon_{\Delta\lambda}$ is only slightly dependent on temperature structure close to the ground and on spectral position within the main thermal infrared window (Figure 1).

2.4.2 Water vapour influence. Water vapour is the dominant absorber within the thermal infrared window from 10 to 13 μm wavelength. It is not possible to reduce its influence strongly by choosing narrow spectral intervals, since the main absorption is not due to single water vapour lines but to the so-called water vapour continuum, often termed e-type absorption with reference to the vapour pressure e dependence. The origin of this absorption, either wings of distant lines or water vapour polymers, is still not known.

As both absorption within the atmosphere and the different emission temperatures determine ΔT we should expect a strong dependence of the water vapour contribution to ΔT on temperature structure. This is clearly shown in Figure 2 (modified after Stork, 1984), where ΔT for strong inversions nearly vanishes and also loses water vapour content dependence while water vapour dependence is very strong for heated surfaces (daytime dry land surface). Another fact from Figure 2 should be stressed: even in midlatitude atmospheres with water vapour content < 2.5 g.m^{-2} ΔT may vary between daytime and nighttime conditions by up to 8 K. Figure 2 also indicates the advantage of a two channel or split-window approach. The different water vapour content dependence allows an approximate calculation of ΔT without ground truth or knowledge of climatology.

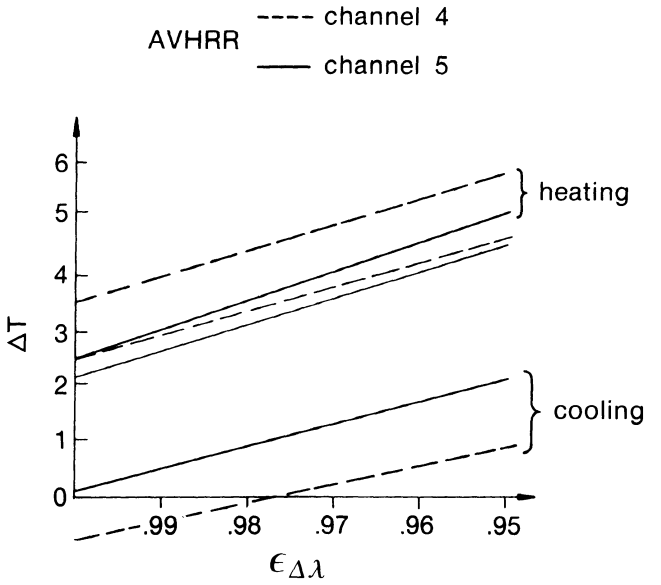

Figure 1. Temperature correction ΔT in K in a 45°N standard atmosphere as a function of mean spectral surface emissivity $\varepsilon_{\Delta\lambda}$ for the wavelength band of a radiometer channel. Extreme temperature structure variations at the ground (10 K heating, 10 K cooling) do not change slopes appreciably (Stork, 1984).

2.4.3 Temperature structure influence. The lower the temperature at which an atmospheric absorber emits (if compared to T_s), the higher the ΔT. Therefore, whenever atmospheric absorbers mask the surface, we need information on the temperature structure of the atmosphere in order to estimate the absorber's influence on remote surface temperature determination. Since water vapour content is strongly concentrated near to the ground and since it is the most important absorber in this context, the near surface temperature structure should be investigated first.

The main results of systematic simulations of lower tropospheric temperature variations are:

- temperature inversions at the surface reduce ΔT, eventually giving $\Delta T \leq 0$ for strong inversions (see also Figure 2);
- heated surfaces lead to a strong enhancement of ΔT, if compared to corresponding atmospheric temperature structure at adiabatic lapse rates;
- both above effects increase with increasing absorption, i.e. in channel 5 of the AVHRR, $\Delta T < 0$ is reached earlier at increasing inversion strength;
- in many cases ΔT varies by more than 2 K between daytime and nighttime vertical temperature profiles, thus rendering the application of

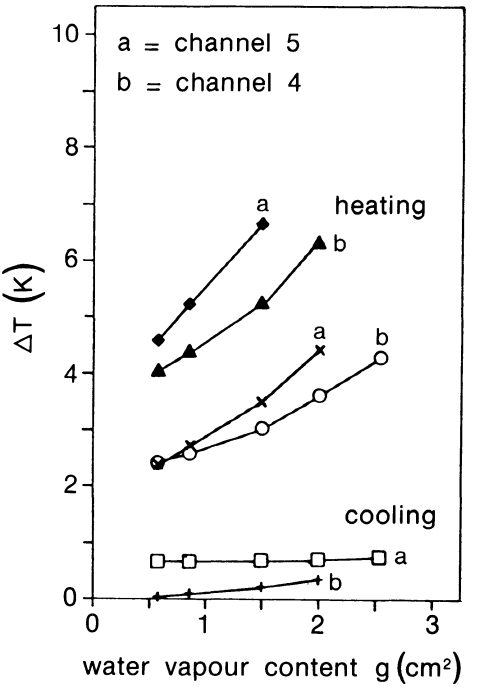

Figure 2. Temperature correction ΔT as a function of water vapour column content for a 45°N standard atmosphere, AVHRR channels 4 and 5, as well as surface heating and surface cooling by 10 K; nadir view; water surface emissivity ε_λ.

a mean ΔT to a one-channel brightness temperature T_B of little use;
- determination of remote surface temperature is most difficult for daytime situations over heated land surfaces.

The second effect of temperature structure, if ordered corresponding to importance for surface temperature determination, is the low temperature in the upper troposphere and lower stratosphere. Optically thin cirrus clouds, often not detected, and stratopheric aerosol layers, therefore, become most important. They reduce the first term in Eq.(1), but however do not add much to the second term ($B_\lambda(T) \sim T^4$ near 10 µm wavelength and thus very small at -50°C), at the low temperatures mentioned.

2.4.4 Off-nadir view. Imaging infrared radiometers like those onboard METEOSAT or NOAA-N look onto the Earth's surface at different angles, changing from pixel to pixel. Therefore, ΔT must be different for all pixels even with a fixed vertical structure of the atmosphere and fixed surface properties. While all results up to now were for the nadir view, Figure 3 demonstrates the ΔT increase for the off-nadir

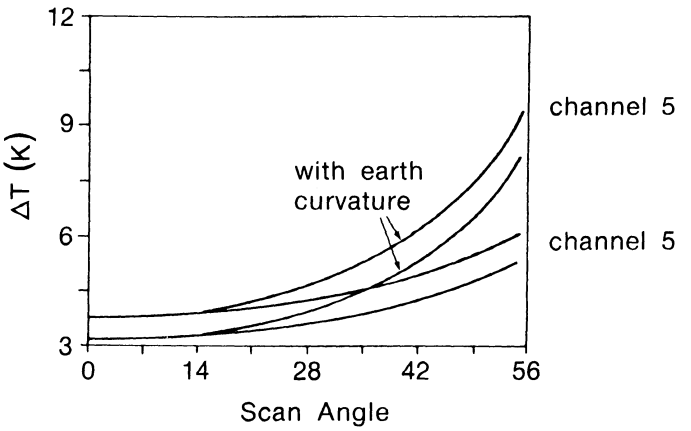

Figure 3. ΔT as a function of the scan angle (off-nadir) for the split-window channels of the AVHRR both for a flat surface and the Earth's surface.

view also.

The curves, shown for the split-window channels of NOAA-7, also account for the sphericity of the Earth. If the curves were plotted as a function of relative airmass m, they would not show a linear dependence. This is for the most part not due to the temperature decrease with height in the troposphere but to the compensational effect of the second term in Eq.(3). $\Delta T \sim m^n$ with $n < 1$ leads to a doubling of ΔT (nadir) at $m > 2$, which is however, because of the sphericity of the Earth, already reached at about 50^o scan angle, an angle inside the $\pm 54^o$ cross-track scan of the AVHRR.

2.4.5 Aerosol particle effects. Aerosol particles scatter and absorb; thus it is more difficult to understand their impact on ΔT than that of gases. Even as pure scatterers they would increase ΔT, because the compensating second term in Eq.(3) then vanishes. The typical value of total aerosol optical depth τ_a (see Eq.(2)) in the visible (0.55 μm wavelength normally used as a reference wavelength) is 0.2. However, $\tau_{a,0.55}$ may reach 1.0 during Saharan dust storms or in metropolitan areas. At thermal infrared window wavelengths $\tau_{a,0.55}/\tau_a \approx 5$, the exact relation depending mainly on the size of the particles. Also the partitioning of extinction into scattering and absorption, and thus the chemical composition, play an important role since the wavelength dependence of $\Delta T/\Delta\tau_{a,0.55}$ is not well known in the thermal infrared window. We may expect the failure of the split-window technique for aerosol effect correction and thus need additional channels for a satellite-alone retrieval of T_s.

Since the vertical distribution of aerosol particle number density is even more variable than that of water vapour density, the aerosol particle contribution to ΔT may vanish as for clear polar air or may

be as important as water vapour in cases with high lying aerosol layers. For cases where most of the aerosol load is confined to the planetary boundary layer - the standard case - $\Delta T/\Delta\tau_{a,0.55} \cong 5$ K per unit optical depth; i.e. typically .5 K must be added to satellite brightness temperatures to compensate for the aerosol effect. The exact value of $\Delta T/\Delta\tau_{a,0.55}$ additionally depends rather strongly on relative humidity and water vapour column content.

2.4.6 Optically thin clouds. Any surface temperature algorithm applied so far must rely on a cloud detection procedure applied before the temperature algorithm. Because of a frequent failure of cloud detection algorithms for optically thin or sub-pixel sized clouds, the possible influence of thin cirrus clouds on brightness temperatures is shown as an example. Figure 4 from Manschke (1985) also includes aerosol effects. It is clearly seen that

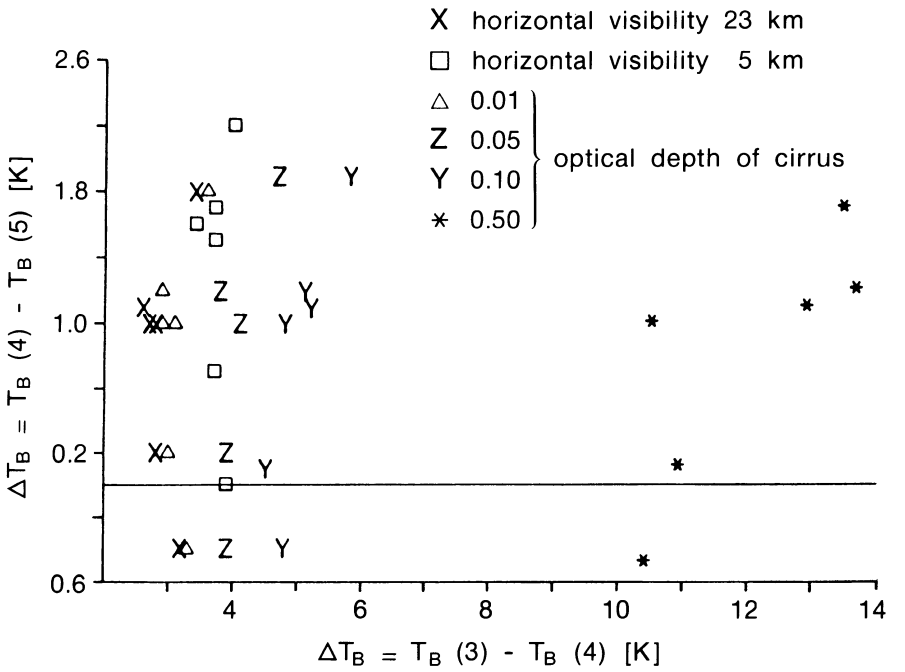

Figure 4. Brightness temperature differences $\Delta T_B = T_B(3) - T_B(4)$ versus $\Delta T_B = T_B(4) - T_B(5)$ for 6 atmospheres (45°N summer, autumn, winter; subarctic summer and winter; tropics 10°N) and at 6 cirrus or aerosol disturbances as indicated.

- the difference $\Delta T_B = T_B(3) - T_B(4)$ of channels 3 at 3.7 μm and 4 at 11 μm of the AVHRR is well suited for a cloud detection;
- aerosol effects at a horizontal visibility change from 23 to 5 km are smaller than those for 0.05 optical depth of a cirrus at 10 km height;
- aerosol effects also have more impact on $T_B(3) - T_B(4)$ than on $T_B(4) - T_B(5)$;
- differences among atmospheres dominate ΔT_B for $\tau_{cirrus} \leqq 0.1$, thus offering T_S determination through thin cirrus as shown by Manschke (1985) for water surfaces.

Different procedures for detecting thin and sub-pixel sized clouds as well will be presented in section 3.5.

2.4.7 Other influences. The thermal infrared window from 10-13 μm as well as other smaller thermal infrared windows are not free of absorption by other gases than water vapour. For well-mixed gases like carbon dioxide (CO_2), methane (CH_4) and nitrous oxide (N_2O), the influence has been taken into account for the simulations presented. They also pose no severe problems when applying T_S retrieval algorithms to satellite data. Depending on the satellite radiometer channel, ozone may also be important for the exact ΔT (Grassl and Koepke, 1980).

3. ALGORITHMS

It is now common practice to call an equation coupling satellite radiances and atmospheric parameters via an empirical or semi-empirical though simple relation an algorithm. Despite a possible success when "playing" with brightness temperatures or their differences during the search for a retrieval procedure or an algorithm, one should normally start with the basic equation, simplify it and then adjust some parameters by validating remote measurements with in-situ data whenever possible. This way will be chosen for the multi-channel approach, but one-channel surface temperature estimation will be considered first.

3.1 T_S from a Single Channel

From the variability of the temperature correction ΔT, shown in section 2.4, it follows that the surface temperature T_S from a single channel will be least accurate over heated land surfaces at high relative humidity and high level turbidity, if only climatological corrections ΔT are applied to the satellite data. Under these circumstances and for the outer parts of the swath $\Delta T \gtrsim +10$ K is not rare.

On the other hand, for a nearby lake in spring, as shown by McClain (1986), $\Delta T \gtrsim 0$ K may be correct. Thus the satellite brightness temperature map often smoothes horizontal surface temperature differences. How should one then proceed, if only one channel is available? The answer is: Use as much additional information as is available. This additional information may be
- radiosonde data;

- short-term temperature profile forecasts;
- routine air temperature (2 m height) observations;
- bulk temperature observations in lakes and rivers;
- physical models of relative near surface temperature profiles as a function of season and daytime;
- calibration by a multi-channel satellite radiometer (for example AVHRR for METEOSAT as shown by Singh et al., 1985).

In this context the impact of the emissivity difference $\Delta\varepsilon_\lambda = 1-\varepsilon_\lambda$ over land is often exaggerated, since over vegetated surfaces it is small; even if for a tiny surface element (dry leaf) $\Delta\varepsilon_\lambda$ may reach 0.1, the roughness of all vegetation causes the mean emission of a satellite pixel to approach the blackbody emissivity: a wheat field is composed of many "black" holes. However, this discussion leads us to the difficulty of defining the mean surface temperature of rough surfaces. While we have no difficulties for smooth water surfaces (it is the skin temperature with radiation originating from the uppermost micrometers), we may still call it the surface temperature of a forest, although all portions of trees, the grass and the ground below contribute in varying amounts.

ΔT is more strongly influenced by heating or cooling of surfaces relative to the atmospheric temperature above the surface layer than by the emissivity deficit $\Delta\varepsilon_\lambda$.

3.2 T_s from at Least Two Channels

Firstly, by simplifying Eq.(3) the basic two-channel or split-window algorithm will be derived, following McMillin (1975). Neglecting the third term in Eq.(3), the contribution by reflecting atmospheric emission, thus setting $\varepsilon_\lambda = 1$ and applying the mean value theorem, we obtain:

$$I_\lambda^+ = B_\lambda(T_s)e^{-\tau_\lambda^*} + \bar{B}_\lambda(\bar{T})(1-e^{-\tau_\lambda^*}) \qquad (11)$$

with $\bar{B}_\lambda(\bar{T})$ = mean spectral radiance of the atmosphere, Planck's function at an appropriate temperature $\bar{T}$ for a given transmission $t = e^{-\tau_\lambda^*}$.

For two channels, i.e. two different wavelength intervals, the spectral dependence of upward radiance I_λ^+ and the source function, Planck's function $B_\lambda(T)$, must be introduced, here by a Taylor expansion truncated after the first expansion term

$$B(\lambda_r,T) \simeq B_\lambda(T) + \frac{\partial B_\lambda(T)}{\partial\lambda}(\lambda_r-\lambda) \qquad (12a)$$

and

$$I^+(\lambda_r) \simeq I_\lambda^+ + \frac{\partial I_\lambda^+}{\partial\lambda}(\lambda_r-\lambda) \qquad (12b)$$

where λ_r is a reference wavelength within the 10-13 µm window. Since T_s, $\bar{T}$ and T_I (reached by inversion of I_λ^+) are close together for the

10-13 μm range and thus will not change appreciably with λ, we put

$$\frac{\partial I_\lambda^+}{\partial \lambda} \approx \frac{\partial B_\lambda(\bar{T})}{\partial \lambda} \approx \frac{\partial B_\lambda(T_s)}{\partial \lambda} \approx \frac{\partial B_\lambda(T_I)}{\partial \lambda} \tag{13}$$

Eq.(11) for any radiometer channel wavelength interval $\Delta\lambda_i$ within the 10-13 μm range is then simplified into (Eq.(11) into (12b); Eq.(12a) into the result)

$$I^+_{\Delta\lambda_i} = B_{\lambda_r}(T_s) e^{-\tau^*_{\lambda_i}} + \bar{B}_{\lambda_r}(\bar{T})(1-e^{-\tau^*_{\lambda_i}}) \tag{14}$$

Writing Eq.(14) for two channels using $B_{\lambda_{1r}}(\bar{T}) \approx B_{\lambda_{2r}}(\bar{T})$, which is proved by radiative transfer calculations, subsequent subtraction and resolving for $B_{\lambda_r}(T_s)$, gives

$$B_{\lambda_r}(T_s) = I^+_{\lambda_{1r}} + \frac{1 - e^{-\tau^*_{\lambda_1}}}{e^{-\tau^*_{\lambda_1}} - e^{-\tau^*_{\lambda_2}}} (I^+_{\lambda_{1r}} - I^+_{\lambda_{2r}}) =$$

$$= I_1^+ + \gamma (I_1^+ - I_2^+) \tag{15}$$

If this equation is converted into an equation for brightness temperatures T_B (see Eq.(5)), the basic version of the split-window algorithm is found

$$T_s = T_B(1) + b\, T_B(1) - T_B(2) + a \tag{16}$$

where the constant a accounts for errors due to the simplifications (Eqs.(11), (12), (13) and $B_{\lambda_{1r}} = B_{\lambda_{2r}}$) used to derive Eq.(16) from Eq.(3).

3.3 Achievements of the Split-Window Algorithm over Water

The algorithm (16) has been used primarily for sea surface temperature determination and numerous coefficients have been derived by different groups (examples are Strong and McClain (1984; Llewelyn-Jones et al. (1984); Schlüssel et al. (1987)). The differences in coefficients a and b mainly stem from the set of atmospheres and in-situ data used, and the accuracy and the quantity with which a comparison has been made, for instance bulk or skin temperature measured from a buoy or from a ship. It has also been shown that a regional algorithm is superior to a global, if only two channels are available (Llewelyn-Jones et al., 1984). The accuracies achieved by the two NOAA satellites with a split-window (NOAA 7 and NOAA 9) are best documented by showing the increased accuracy during the buoy-satellite matchups in Figure 5 and the accuracies after classification into daytime, nighttime and humidity

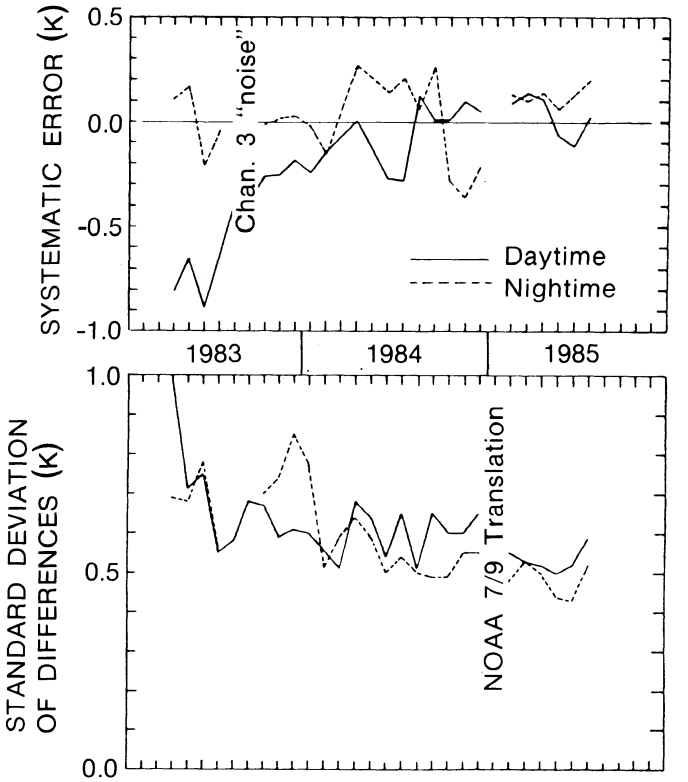

Figure 5. Systematic error and standard deviation monthly means between satellite derived and buoy bulk temperatures as a function of time for the split-window technique. Nighttime temperatures also use channel 3 and thus a modified algorithm.

intervals in Table II (taken from WCP-110, 1986).

3.4 Algorithms over Land?

Knowing the main result for water surfaces, namely a temperature nearly free of systematic errors and with only 0.5 K rms error, we ask whether the split-window algorithms may be applied to land surfaces. The answer is no, since the following facts must be taken into account:

- spectral emissivity changes from one surface type to the next, causing a ΔT_B of the same magnitude as humidity (see Table IIb) and thus leading to a false ΔT;
- cloud detection during daytime is exceptionally difficult over bright surfaces like snow or sand dunes;
- strong near surface heating or cooling is only partly accounted for by two spectral channels.

TABLE IIa
February - August 1985: matchup statistics for day and night and for different areas

REGION	DAY			NIGHT		
	No.	Bias	RMSD	No.	Bias	RMSD
World	1625	+0.01	0.55	1042	+0.12	0.48
W. Trop. Pac.	189	-0.02	0.47	102	+0.22	0.40
E. Trop. Pac.	433	-0.15	0.55	290	+0.08	0.41
Trop. Atl.	424	+0.08	0.51	277	+0.12	0.51
Trop. Ind.	277	-0.03	0.50	163	+0.11	0.46
N. Atl. & Pac.	208	+0.18	0.60	115	+0.18	0.54
N. Pac.	112	+0.25	0.65	74	+0.16	0.59
N. Atl.	96	+0.10	0.53	41	+0.23	0.46
Southern Ocean	139	+0.08	0.63	113	+0.11	0.44

TABLE IIb
February - August 1985: matchup statistics by moisture class, indicated by the brightness temperature difference classes

MOISTURE (Tropical Oceans)	DAY			NIGHT		
	No.	Bias	RMSD	No.	Bias	RMSD
$0^\circ < T_4 - T_5 < 1^\circ$	500	-0.08	0.47	218	+0.16	0.47
$1^\circ < T_4 - T_5 < 2^\circ$	694	+0.00	0.56	553	+0.09	0.46
$2^\circ < T_4 - T_5 < 3^\circ$	69	-0.01	0.61	38	-0.01	0.52

My proposal for a procedure for land surface temperature determination from two or more satellite brightness temperatures, therefore, was:

1) determine cloud-free parts;
2) use the split-window algorithm (16) over water surfaces within the area envisaged;
3) inter- and extrapolate the "water surface" atmospheric correction;
4) derive an additional correction from the brightness temperature difference between water surfaces and a land surface pixel for the channels available;
5) choose after adding the second correction the highest temperature to reach a good estimate of the surface temperature.

3.5 Application of the Proposed Procedure to ALPEX SOP Satellite Data

During one of the special observing periods (SOP) within the ALPEX (Alpex Experiment) rather cloudfree satellite data during day- and nighttime could be acquired on the 25th and 26th March 1982. For this

time the procedure outlined above is applied to NOAA 7 data by Stork (1984). Since the images cover a major portion of the Alps, this was a hard test as far as cloud clearing and interpolation were concerned.

Step 1: cloud clearing. Four different procedures were applied simultaneously to daytime images. They are shown in Table III.

TABLE III
Cloud clearing thresholds (cloudy if above this threshold)[1]

Water surfaces	Snowfree land surfaces
Channel 1: $A_S \geq 0.15$[2]	$A_S > 0.15$
Channel 2: $A_S \geq 0.15$	$A_S > 0.24$
$T_B(3) - T_B(4) > 3$ K	$T_B(3) - T_B(4) > 5$ K
$T_B(4) - T_B(5) > 1.7$ K	$T_B(4) - T_B(5) > 1.9$ K

[1] all thresholds were chosen interactively at an image processing system.
[2] A_S = albedo.

Nighttime cloud clearing, rather easy over water, as shown by Olesen and Grassl (1985), is more difficult over land. Therefore, no table similar to Table III can be shown.

Step 2: surface temperature over water surfaces. For midlatitude atmospheres and the NOAA 7 satellite the split-window algorithm (16) for water surfaces is, following Jürgensen (1984)

$$T_S = 3.345\ T_B(4) - 2.363\ T_B(5) + 5.74\ \text{K} \tag{17}$$

This algorithm was applied to all big lakes within the scene and to the Adriatic Sea.

Step 3: inter- and extrapolation. Before an interpolation the atmospheric corrections over water ranging from 2 to 3 K for all big lakes and the Adriatic Sea were spatially averaged. Thus the noise in single ΔTs due to the 0.12 K noise equivalent $\Delta T_S'(NE\Delta T)$ of the satellite radiometer was strongly suppressed. The rather small number of lakes does not allow a polynomial of higher order to be fitted to the water surface $\Delta T_S'$. Therefore, only a first and second order polynomial were chosen. Even the second order polynomial led to strong errors within the extrapolation area. Whenever extrapolation is necessary we have chosen as atmospheric correction ΔT for the image coordinates x,y and for channel i

$$\Delta T_i(x,y) = a_{1_i} x + a_{2_i} y + a_{3_i} \tag{18}$$

leading to a first approximation of surface temperature

$$T_{S_1}(x,y) = T_B(i) + \Delta T_i(x,y) \tag{19}$$

T_{s_1} still contains errors due to the near surface heating or cooling as well as to emissivity changes.

Step 4: additional correction derived from the water-land contrast. As shown in section 2.4 the heating or cooling of land surfaces increases or decreases the correction ΔT. For a midlatitude atmosphere ($45^{o}N$) the additional correction may reach 3 K for a +20 K change in surface temperature. From model simulations we found for channels 4 and 5:

$$\Delta T_4' = 0.14\ \Delta T_{s_1} \quad (4)$$
$$\Delta T_5' = 0.22\ \Delta T_{s_1} \quad (5) \qquad (20)$$

These relations also hold for cooling, i.e. for negative temperature differences ΔT_{s_1}, if ΔT_{s_1} is the difference between T_{s_1} and the interpolated water surface temperature. After this correction the second approximation for T_s is reached

$$T_{s_2}(i) = T_B(i) + \Delta T_i(x,y) + \Delta T_i' \qquad (21)$$

$\Delta T_4'$ is shown in Figure 6.

Step 5: correction of emissivity changes. The effects of unknown surface emissivity and thus of unknown spectral dependence can only be removed partially. After applying corrections (19) and (21) to channel 4 and 5 one should choose the channel with higher temperature, since this channel should be the channel nearer to a blackbody emission. Choosing the higher temperature we arrive at T_s, the quantity desired. However, whenever the difference of T_s between both channels exceeds 1 K, pointing to $\Delta\varepsilon_\lambda > 2\%$, we discard this value and classify the pixel as cloud contaminated.

T_s from Figures 7 and 8a,b contains a wealth of information for climatologists.

3.6 Error Analysis

The following error sources should be discussed:
- conversion from counts to brightness temperatures;
- split-window algorithm for water surfaces (Eq.(17));
- interpolation errors (Eq.(18));
- water-land differences (Eq.(20));
- remaining emissivity difference.

The conversion from counts with a 10 bit resolution to brightness temperature is, according to Singh (1984), accurate to 0.01 K and thus errors are negligibly small. The radiometric noise expressed by the noise equivalent temperature difference ($NE\Delta T = 0.12$ K for channels 4 and 5 of AVHRR and for the 270 to 300 K range) is easily suppressed by

spatial averaging. The split-window algorithm combining errors due to changing atmospheric structure not resolved and the NEΔT after spatial averaging is affected by a 0.5 K rms error (see Table II). If - as done here - T_S is determined on a pixel by pixel basis the combination leads to a slightly higher standard error for water surface temperature determination.

The interpolation error strongly depends on the number of water surfaces found in a scene. For 23 lakes in the chosen scene and the first order polynomial (18) the error of the atmospheric correction ΔT for water surfaces reaches 0.6 and 0.85 K for channel 4 and 5, respectively.

The adoption of this interpolated correction for synthetic water surfaces, $\Delta T_i(x,y)$, as a first approximation (Eq.(19)) for land surface temperature, enhances the rms error from 0.51 K for lakes to 0.8 K over land if the more transparent channel 4 is chosen. This error would increase to 1.0 K for channel 5. One should, however, be aware of the large systematic errors left because of heated or cooled surfaces and emissivity changes. These systematic errors are reduced by steps 4 and 5 (section 3.4). On the other hand, step 4 increases the rms error to 0.9 K for channel 4 and 1.1 K for channel 5.

The discussion of errors due to surface emissivity changes is more difficult. Since $\Delta\varepsilon_{\Delta\lambda} = 0.02$ is the upper limit for differences within the 10-13 µm window for smooth rock surfaces and since this would cause a systematic underestimate of T_S by about 1 K, we expect over vegetated surfaces with $\varepsilon_{\Delta\lambda} > 0.95$ and $\Delta\varepsilon_{\Delta\lambda} < 0.02$ an additional systematic error $\leq$ 1 K which, however, is reduced by step 5 where the higher temperature of both channels is chosen.

An accuracy of 1-2 K for T_S of land surfaces is a step forward at least for daytime situations, where the atmospheric masking may reach 10 K.

A verification of the approach described is only possible by radiometric measurements from masts and airplanes. This has been shown to be successful for ocean surfaces (Schlüssel et al., 1987) by measurements from a ship, where by a combination of satellite radiometers a 0.3 K rms error was also reached.

3.7 The Daily Temperature Amplitude

The climatologist is sometimes even more interested in daily temperature amplitudes ΔT_D than in T_S, because they are an indication for evaporation and thus help in sensing latent heat fluxes remotely. Already before an application of the approach discussed above for remote land surface temperature determination we had derived ΔT_D for the ALPEX scenes used so far (Grassl et al., 1985).

In the inner Inn Valley, at Schwaz in the Tyrol, we could show by using ground observations and radio soundings that ΔT_D (Figure 9) is accurate to at least 2 K without any atmospheric correction in a valley wind system. The time of the NOAA-7 satellite overpasses at approximately 2.30 a.m. and p.m. guarantees observations at the daily temperature maximum and - best for valleys with a valley wind system -

very near to the temperature minimum. Under calm conditions, however, with strong heating during daytime, the procedure outlined in section 3.4 must be applied especially for the daytime overpass (see Figure 2)

3.8 Further Improvements

Recently, Schlüssel (1987) has demonstrated that a combination of two radiometers onboard the NOAA satellite series, namely the AVHRR and the HIRS (High Resolution Infrared Sounder) improves not only temperature and humidity profiles but also surface temperature over water surfaces. A 0.3 K rms error was found during a verification cruise in the North-East Atlantic for some case studies. The additional information comes from a 6.3 µm band water vapour channel whose weighting function peaks in the lowest troposphere and from three 15 µm-CO_2 channels peaking in the lower troposphere and at the ground. Especiall the algorithm over big lakes and marginal seas would gain in accuracy by introducing the combined algorithm which also accounts for changing coefficients at different viewing angles. However, the latter improvement is also possible for the split-window algorithm (16). Despite the higher accuracy demonstrated for marginal seas there are still extreme conditions (McClain, 1986) in spring over the American big lakes where the improved algorithm failed. Therefore, it might be dangerous to tak 0.5 K rms error for granted over lakes as done in section 3.6.

REFERENCES

Grassl, H. and Koepke, P., 1981: 'Corrections for atmospheric attenuation and surface reflectivity in satellite-borne SST measurements', in Oceanography from Space, Plenum Press, 97-107.

Grassle, H., Stork, T. and v. Rüsten, C., 1985: 'Daily temperature amplitude at the surface from NOAA-7', Zbornik Meteoroloskih i Hydroloskih Radova, 11, 36-39.

Jürgensen, A., 1984: 'Bestimmung des Wasserdampfgehaltes der Atmosphäre über dem Ozean aus Satellitendaten', Diploma Thesis, University of Kiel, FRG.

Llewellyn-Jones, S.T., Minnett, P.J., Saunders, R.W. and Zavody, A.M. 1984: 'Satellite multichannel infrared measurements of sea surface temperature of the North-East Atlantic ocean using AVHRR/2', Quart. J. Roy. Met. Soc., 110, 613-631.

Manschke, A., 1985: 'Einfluss dünner Cirren auf den Strahlungshaushal Diploma Thesis, University of Kiel, FRG.

McClain, P., 1986: private communitation.

McMillin, L.M., 1975: 'Estimation of sea surface temperatures from tw infrared window measurements with different absorption', J. Geophy Res., 80, 5113-5117.

Olesen, F.-S. and Grassl, H., 1985: 'Cloud detection and classification over oceans at night with NOAA-7', Int. J. Rem. Sens., 6, 1435-1444.

Schlüssel, P., 1987: 'Infrarotfernerkundung von Oberflächentemperaturen sowie atmosphärischen Temperatur- und Wasserdampfstrukturen'

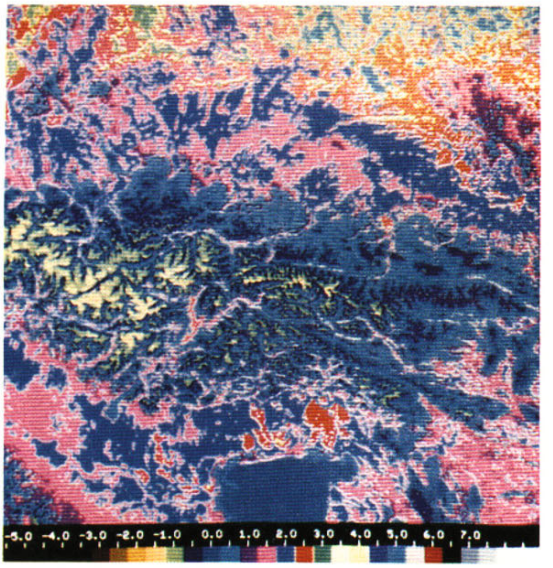

:e 6. $\Delta T_4^{\downarrow}$ for the daytime overpass in steps of 0.5 K indicated .fferent colours (see scale below image).

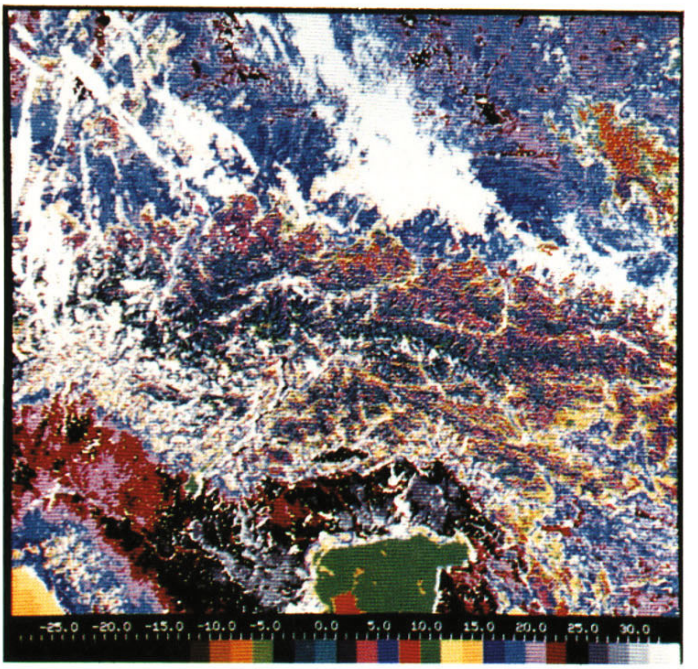

e 7. Surface temperature for the daytime overpass in steps of 25 March 1982, early afternoon); clouds are white.

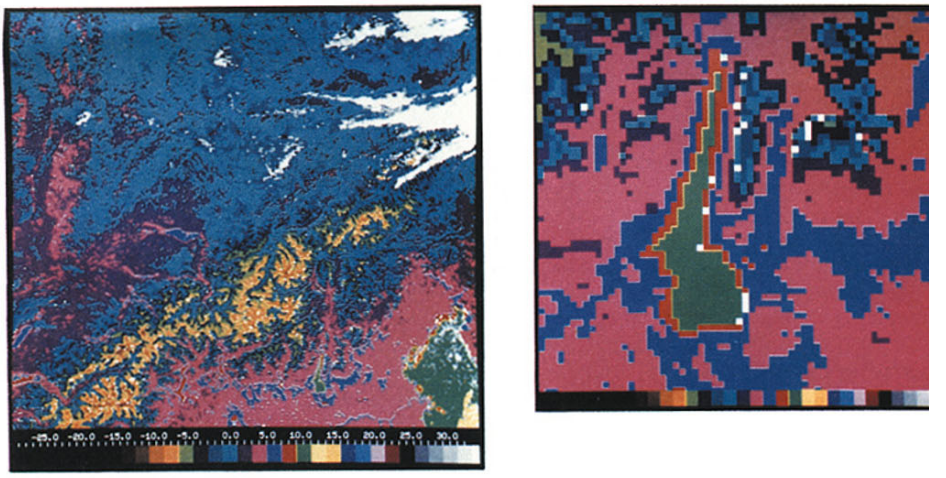

a) b)

Figure 8. Surface temperature for the nighttime overpass in steps of 2 K (26 March 1982, early morning).
a) for the full image;
b) zoom around Lago di Garda, Northern Italy.

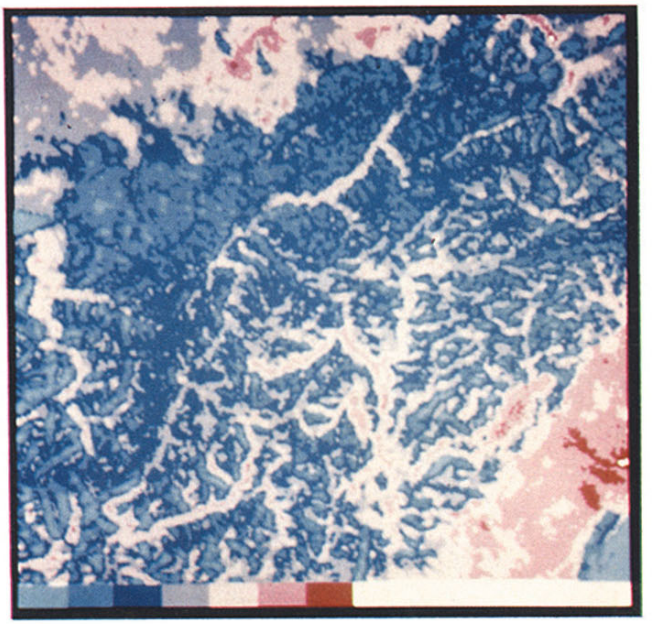

Figure 9. Daily temperature amplitude for parts of the Alps derived solely from brightness temperature differences between 25 March, ∿ 2.30 p.m. and 26 March, ∿ 2.30 a.m.

D. Thesis, University of Kiel. Berichte aus dem Inst. für Meeres-
de, Nr.161, 116 pages.
sel, P., Shin, H.-Y., Emery, W.J. and Grassl, H., 1986: 'Compa-
on of satellite derived sea surface temperatures with in-situ
n measurements', J. Geophys. Res., March issue.
S.M., 1984: 'Removal of atmospheric effects on a pixel basis
m the thermal infrared data from instruments on satellites.
advanced very high resolution radiometer (AVHRR)', Int. J. Rem.
s., 5, 161-183.
T., 1985: 'Bestimmung der Oberflächentemperatur über Land aus
ellitendaten', Diploma Thesis, University of Kiel, FRG.
, A.E. and McClain, E.P., 1984: 'Improved ocean surface tempera-
es from space: comparison with drifting buoys', Bull. Am. Met.
., 65, 138-141.
0, 1986: 'Satellite-derived sea surface temperatures for global
mate applications', Report of the COSPAR int. workshop, Camp
ings, Maryland, USA, 28-31 May 1985; World Climate Programme
ies, WMO, Geneva.